Received: 19 February 2018 | Revised: 3 August 2018 | Accepted: 8 August 2018

DOI: 10.1002/hbm.24359

WILEY

RESEARCH ARTICLE

Structural covariance across the lifespan: Brain development and aging through the lens of inter-network relationships

Katherine S. Aboud[1] | Yuankai Huo[2] | Hakmook Kang[3] | Ashley Ealey[4] | Susan M. Resnick[5] | Bennett A. Landman[6] | Laurie E. Cutting[7]

[1]Department of Special Education, Vanderbilt Brain Institute, Vanderbilt University, Nashville, Tennessee

[2]Department of Electrical Engineering and Computer Science, Vanderbilt University, Nashville, Tennessee

[3]Department of Biostatistics, Vanderbilt University, Nashville, Tennessee

[4]Department of Neuroscience, Agnes Scott College, Decatur, Georgia

[5]National Institute on Aging, Bethesda, Maryland

[6]Departments of Electrical Engineering and Computer Science, Biomedical Engineering, Radiology and Radiological Sciences, Institute of Imaging Science, Vanderbilt University, Nashville, Tennessee

[7]Departments of Special Education, Psychology, Radiology, Pediatrics, Institute of Imaging Sciences, Vanderbilt University, Nashville, Tennessee

Correspondence
Laurie E. Cutting, Education and Brain Sciences Research Lab, Peabody College of Education and Human Development, Vanderbilt University, 230 Appleton Place, PMB 328, Nashville, TN 37203.
Email: laurie.cutting@vanderbilt.edu

Funding information
National Institutes of Health; National Science Foundation, Grant/Award Number: 1452485; National Institute of Neurological Disorders and Stroke, Grant/Award Numbers: N01-NS-9-2320, N01-NS-9-2319, N01-NS-9-2317, N01-NS-9-2316, N01-NS-9-2315, N01-NS-9-2314; National Institute of Mental Health, Grant/Award Number: N01-MH9-0002; National Institute on Drug Abuse; National Institute of Child Health and Human Development, Grant/Award Number: N01-HD02-3343; National Institute on Aging, NIH, Grant/Award Numbers: NCATS/NIH UL1 TR000445, U54 HD083211, R01 HD044073, R01 HD067254, NIH R03EB012461, NIH R21NS064534, NIH R21EY024036, NIH R01EB017230

Abstract

Recent studies have revealed that brain development is marked by morphological synchronization across brain regions. Regions with shared growth trajectories form structural covariance networks (SCNs) that not only map onto functionally identified cognitive systems, but also correlate with a range of cognitive abilities across the lifespan. Despite advances in within-network covariance examinations, few studies have examined lifetime patterns of structural relationships across known SCNs. In the current study, we used a big-data framework and a novel application of covariate-adjusted restricted cubic spline regression to identify volumetric network trajectories and covariance patterns across 13 networks (n = 5,019, ages = 7–90). Our findings revealed that typical development and aging are marked by significant shifts in the degree that networks preferentially coordinate with one another (i.e., modularity). Specifically, childhood showed higher modularity of networks compared to adolescence, reflecting a shift over development from segregation to desegregation of inter-network relationships. The shift from young to middle adulthood was marked by a significant decrease in inter-network modularity and organization, which continued into older adulthood, potentially reflecting changes in brain organizational efficiency with age. This study is the first to characterize brain development and aging in terms of inter-network structural covariance across the lifespan.

KEYWORDS

brain, brain development, lifespan aging, MRI, structural covariance, T1w

1 | INTRODUCTION

Brain development is marked by coordinated structural growth of brain regions, which form what are referred to as structural covariance networks (SCNs; Alexander-Bloch, Giedd, & Bullmore, 2013). In healthy children and adults, the formation of SCNs is dependent on the functional similarity, structural homology, and spatial proximity of the contributing brain areas (Alexander-Bloch et al., 2013; Evans, 2013). While structural correlations are not direct reflections of functional connectivity, or indeed structural connectivity (Alexander-Bloch et al., 2013), SCNs have been proven to provide insight into brain properties of typical and atypical aging, and to some extent correspond with functional and structural connectivity (Gong et al., 2009; Liao et al., 2013). It is consequently not surprising that SCNs parallel known functional networks such as primary sensory, language, and executive networks (Zielinski, Gennatas, Zhou, & Seeley, 2010), are

markers for disease (Seeley, Crawford, Zhou, Miller, & Greicius, 2009), and correlate with individual cognitive variability, including IQ and degree of task expertise (Bermudez, Lerch, Evans, & Zatorre, 2009; Lerch et al., 2006; Lv et al., 2008).

Studies have established a consistent set of individual SCNs (e.g., the auditory SCN is comprised of structurally coordinated regions associated with auditory functions) and probed their relation to subject characteristics (Alexander-Bloch, Raznahan, Bullmore, & Giedd, 2013; Chen, He, Rosa-Neto, Gong, & Evans, 2011; Guo et al., 2015; Montembeault et al., 2012; Zielinski et al., 2010). However, fewer studies have examined how SCN trajectories correlate with one another (e.g., inter-network covariance)—for example, how auditory and visual networks volumetrically change together over development. Importantly, inter-network structural covariance may be a critical missing piece in the understanding of brain development across the lifespan: functional neuroimaging studies suggest that inter-network relationships provide unique insight into typical aging (La et al., 2015), as well as the characteristics of neurobiologically vulnerable populations (Chan, Park, Savalia, Petersen, & Wig, 2014; Tost, Bilek, & Meyer-Lindenberg, 2012). In this study, we used a big-data framework and novel application of covariate-adjusted restricted cubic spline regression to characterize the inter-network volumetric covariance patterns of 13 known SCNs across the lifespan in healthy populations (see Figure 1).

1.1 | Typical age trajectories of SCNs

Structural studies show that childhood and adolescence are marked by organized regional development, the organization of which is dependent both on functional groupings (e.g., lower- versus higher-order cortices) and spatial proximity (Alexander-Bloch et al., 2013; Gogtay et al., 2004; Zielinski et al., 2010). Over the course of development into young adulthood, covariance patterns shift from local to more distributed topologies, with increased communication across networks with age (Fair et al., 2009; Zielinski et al., 2010). The transition from adolescence to young adulthood additionally includes global synaptic pruning processes that lead to the establishment of stable, young adult patterns of covariance (Arain et al., 2013; Zielinski et al., 2010). The transition from young to middle adulthood (~30–55) marks a "shrinking" of connections within expected SCNs (i.e., intra-network connections) (Gong et al., 2009; Li et al., 2013; Montembeault et al., 2012), and a broadening of functional and structural interactions across networks (i.e., inter-network connections; Chen et al., 2011). This pattern of desegregation, in which global communication across networks is preferred, continues into late adulthood (Chen et al., 2011; Li et al., 2013; Montembeault et al., 2012). For example, in the only study to date that has examined any metric of structural inter-network relationships, Chen et al. (2011) compared cortical thickness covariance in older versus younger adults, and found age-related increases in the preference for inter- versus intra-network covariance in older adults. These results parallel functional MRI studies which have found that aging corresponds with disruption within expected functional networks within subjects, particularly associative networks (Siman-Tov et al., 2016), and increased cross-talk between networks—a pattern thought to reflect decreased neural efficiency (Chan et al., 2014). Notably, while there are significant differences in the specific characteristics of SCNs across the lifespan, a comparison of studies reveals core SCNs that are seen in populations during early development, young adulthood, and older adulthood, including primary sensory networks (auditory, visual, and sensorimotor), frontal networks, and networks related to the default mode network (DMN) (Chen et al., 2011; Geng et al., 2016; Li et al., 2013; Zielinski et al., 2010).

Age-related structural differences can consequently be described through measures of modularity. In the context of structural covariance and brain growth patterns, regions (or networks) can be clustered into groups of regions with similar growth patterns. Modularity is the degree to which a region "prefers" its cluster relative to regions outside of its cluster (Sporns & Betzel, 2016; see Supporting Information Figure S1 for examples in the current pipeline). Importantly, the formation of sub-groups along the continuum of modularity can either reflect *organized* or *disorganized* groupings, in which healthy organization preserves high modularity between functional, homotopic, and spatially proximal groupings (Alexander-Bloch et al., 2013), though many studies of brain modularity limit groupings to hypothesized organization strategies. Disruption of organized modularity is associated with a number of neurodegenerative diseases (Hohenfeld, Werner, & Reetz, 2018), particularly Alzheimer's Disease (Brier et al., 2014), as well as neural health in typical aging (Chan et al., 2014),

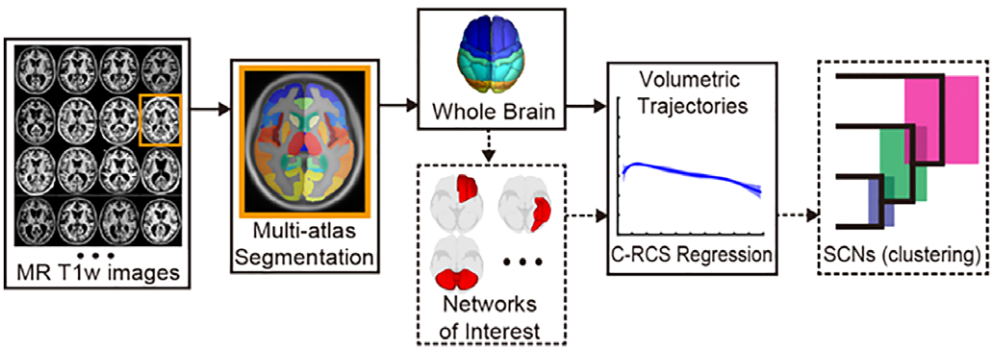

FIGURE 1 Analytical pipeline. Analysis included multi-atlas segmentation of n = 5,019 images and subsequent division into 13 networks of interest, TICV-correction of gray matter volumes, growth curve fitting using a covariate-adjusted restricted cubic spline regression, and hierarchical clustering analysis to identify inter-network correlations [Color figure can be viewed at wileyonlinelibrary.com]

leading some to suggest that the metric of modularity, and its underlying implication of global brain organization, is in fact a key predictive and diagnostic biomarker of neurodegenerative diseases (Brier et al., 2014; Hohenfeld et al., 2018), and brain health over aging more generally (Chan et al., 2014). Previous work suggests that brain organization can be described through two primary metrics: (a) the parcellation characteristics of network sub-groupings (e.g., whether networks that are functionally or spatially related are correlated with each other), and (b) the lateral coordination (LC) of homotopic brain areas (e.g., how closely left and right hemisphere homologs correlate with each other).

The current study aimed to identify lifespan patterns of inter-network covariance in healthy populations along three primary dimensions of efficient brain organization: modularity, parcellation, and LC. From this conceptual framework, we hypothesized that inter-network modularity would vary significantly across developmental age groups (see Figure 2). Specifically, we anticipated that early life would be marked by efficient network organization (as reflected by high modularity with organized inter-network groupings), while later adulthood would show a shift to inefficient network organization (as reflected by low modularity and disorganized inter-network groupings). While our examination was cross-sectional and, consequently, does not directly reflect growth/decline processes within individuals (see Sections 4 and 5), the present findings fill a critical gap between previous studies that have been restricted to regional and whole brain examinations of brain development. The current study provides a new systems-level framework in which to examine changes in clinical and nonclinical populations.

2 | METHODS

2.1 | Participants

Data included n = 5,019 (2,319 females; age range = 7–90 years) healthy subjects with T1w 3D MR images from nine data sets (see Table 1 and Figure 3). Only subjects that were marked as controls in each dataset were used in the present project, with the exception of children with a diagnosis of attention-deficit/hyperactivity disorder or dyslexia. Subjects with autism, mild cognitive impairment, Alzheimer's disease, or psychiatric diagnoses were excluded.

2.2 | Segmentation

A multi-atlas segmentation framework was used to automatically segment each T1-weighted image; 45 atlases were nonrigidly registered (Avants et al., 2008) to a target image (i.e., the subject's T1 image) and nonlocal spatial staple (NLSS) label fusion (Asman et al., 2014) was used to fuse the labels from each atlas to the target image under the

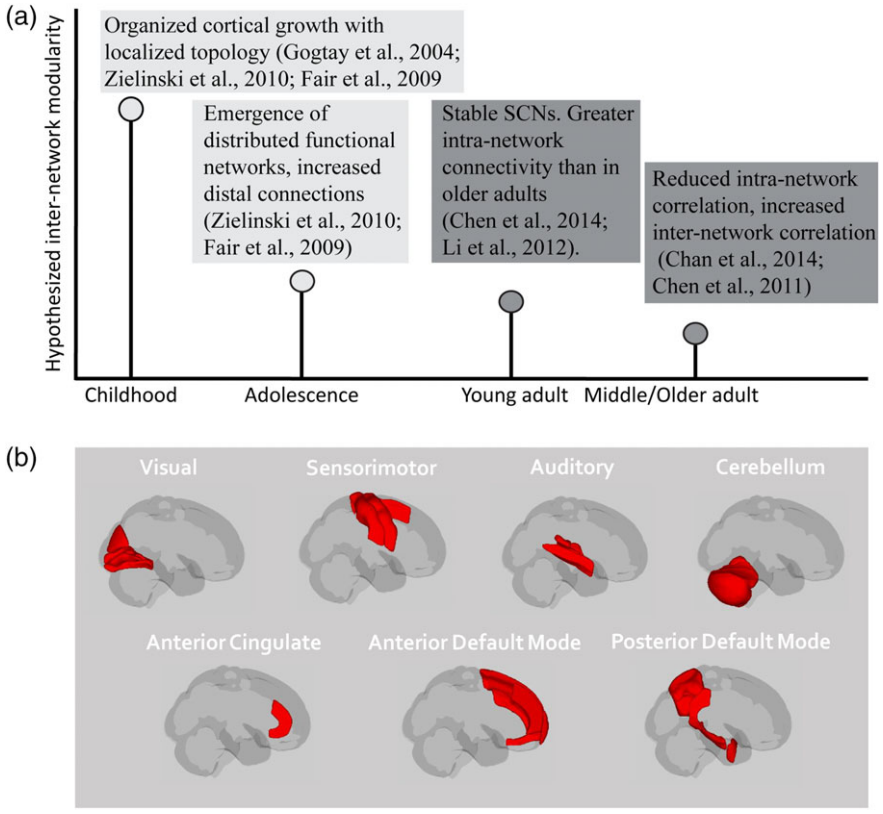

FIGURE 2 Hypotheses and networks of interest (NOIs). (a) selected studies suggest that there are age-related differences in regional structural covariance networks (SCNs), which the present study extended to inter-network hypotheses. Current studies of structural covariance are restricted to either early (light gray) or later (dark gray) life examinations, and only one study that we are aware of (Chen et al., 2011) has examined inter-network structural correlation patterns in any age group. (b) the current study examined 13 core SCNs (left and right of those displayed here, with the exception of the cerebellum) that are seen in development, young adulthood, and later life (see Section 2 for full description). See Table 2 for regions included in each network [Color figure can be viewed at wileyonlinelibrary.com]

TABLE 1 Subject demographics per age group per site

Site	Mean age	7–12	12–19	19–30	30–55	55–75	75–90	Site total
ABIDE	17.2 ± 7.7	145 (28)	248 (49)	126 (17)	42 (4)	1 (0)	–	562 (98)
ADHD-200	11.6 ± 3.3	535 (216)	381 (131)	33 (19)	–	–	–	949 (366)
BLSA	67.8 ± 12.4	–	–	1 (0)	89 (47)	318 (195)	190 (85)	598 (327)
Cutting	12.6 ± 5.0	348 (181)	136 (51)	88 (53)	3 (1)	–	–	575 (286)
Fcon-1,000	28.4 ± 13.7	8 (2)	62 (27)	757 (443)	187 (82)	77 (42)	11 (8)	1,102 (604)
IXI	48.8 ± 16.4	–	–	85 (50)	217 (109)	201 (126)	20 (11)	523 (296)
NDAR	12.2 ± 3.28	139 (69)	122 (62)	5 (2)	–	–	–	266 (133)
NKI Rockland	35.3 ± 21.0	11 (7)	25 (11)	34 (15)	45 (17)	16 (10)	9 (0)	140 (60)
OASIS	44.0 ± 23.0	–	8 (5)	127 (71)	64 (38)	67 (28)	38 (7)	304 (149)
Age total	29.3 ± 22.3	1,186 (503)	982 (336)	1,256 (670)	647 (298)	680 (401)	268 (111)	5,019 (2319)

Parentheses contain number of females.

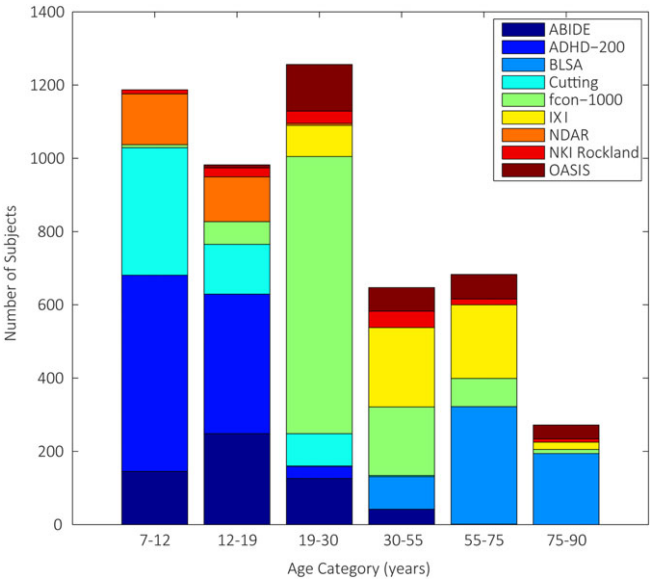

FIGURE 3 Subjects per age group per site. Final subject inclusion numbers after quality control steps show that each age bin was represented by multiple sites, and each site was represented across multiple age bins. See Table 1 for specific number of images per age per site [Color figure can be viewed at wileyonlinelibrary.com]

BrainCOLOR protocol (Klein et al., 2010) (Figure 1). NLSS label fusion uses multiple atlases to "rate" what atlas label each voxel should receive. NLSS improves upon previous multi-atlas segmentation tools by taking into account known anatomical features that can weight individual atlas ratings based on the atlas's alignment with the known structures. Whole brain and regional volume were then calculated by multiplying the volume of a single voxel by the number of voxels from the fused labels in original image space. All segmentations underwent automated and manual quality control (QC) protocols (see below). Notably, multi-atlas segmentation is not sensitive to absolute intensity (Huo, Aboud, Kang, Cutting, & Landman, 2016), and is consequently robust to site-related intensity differences.

2.3 | Network definition

For each subject, the sum gray matter volume (GMV; mm^3) was extracted from voxels within the anatomical regions that fell within 13 previously identified basic SCNs (see Table 2 for anatomical regions). The 13 SCNs examined in the present article have been found to be stable in young adults, and have been previously identified based on data-driven approaches rather than seed selection (see Figure 2; Guo et al., 2015). Similar networks have been observed in (a) early in development (Geng et al., 2016) and (b) in healthy aging (Chen et al., 2011; Li et al., 2013). Networks included: bilateral visual, bilateral auditory, bilateral sensorimotor, cerebellum (CB), bilateral anterior cingulate, bilateral anterior DMN, and bilateral posterior DMN (see Table 2 for regions included in each network). Intra-network relationships for the 13 networks have already been well described (see Chen et al., 2011; Geng et al., 2016; Guo et al., 2015; Li et al., 2013), and in order to reduce data dimensionality and isolate the relationships *between* these specific networks across different ages, intra-network relationships were not considered for the present article. However, as intra-network relationships likely interact with inter-network relationships differentially across the lifespan, characterization of this interaction is an important complimentary question that should be examined by future studies (please see Section 5). Total intracranial volume (TICV) was estimated by SIENAX (Smith, et al., 2001, 2002), part of FSL (Smith et al., 2004), and used to account for overall brain size. TICV has been widely used as a covariate in brain volumetric analyses to control the inter-subject variations in overall brain size (Barnes et al., 2010; Farias et al., 2012; Peelle et al., 2012; Westman et al., 2013; Whitwell et al., 2001).

2.4 | Quality control

All images underwent a rigorous three-part QC protocol. First, images underwent an automated QC check, and images were marked as questionable if their regional volume fell outside of 2.5 standard deviations from the overall population. In parallel, all image segmentations were manually inspected by a trained observer. If images were marked as questionable by either the automated or manual QC pipelines, they were inspected by a second trained observer. If segmentations did not pass QC, the image was excluded from analysis. Final inclusion determinations were made based on discussion.

2.5 | Covariate-adjusted restricted cubic spline

For each network, cross-sectional growth curves were generated for different developmental age ranges (see below) using covariate-

TABLE 2 Regions included in 13 a priori networks

Network name	Regions
Visual	Calcarine cortex
	Lingual gyrus
	Middle occipital gyrus
Auditory	Posterior insula
	Parietal operculum
	Superior temporal gyrus
	Transverse temporal gyrus
Sensorimotor	Postcentral gyrus (medial)
	Precentral gyrus (medial)
	Postcentral gyrus (lateral)
	Precentral gyrus (lateral)
	Supplementary motor cortex
Cerebellum	Cerebellum exterior
	Vermis
Anterior cingulate	Anterior cingulate cortex
Anterior default mode network	Frontal pole
	Medial frontal cortex
	Medial frontal gyrus
	Superior frontal gyrus (medial)
	Superior frontal gyrus (lateral)
Posterior default mode network	Angular gyrus
	Posterior cingulate
	Superior parietal lobule
	Hippocampus
	Entorhinal area

Regions defined from typical structural covariance networks identified as consistent in Guo et al. (2015).

adjusted restricted cubic spline (C-RCS) regression (for full description of method see Huo et al., 2016). Briefly, in RCS regression, cubic splines are used to model nonlinear relationships between variables x and y by deciding the connections between K knots. Here, knots were defined at four equally spaced percentiles per age bin, which is an appropriate number of control points for moderate to large sample sizes (Harrell, 2015). Additionally, a linear constraint is introduced to address the poor behavior of the cubic spline model in the tails, ensuring that the fit is not influenced by edge effects (Harrell, 2015). Using the same principle, C-RCS regression extends the RCS regression by allowing traditional covariates and interaction effects consistent with the general linear model approach. The model of gray matter volume over age consequently included TICV-corrected network volume as the dependent variable, and age, sex, and field strength as the independent variables (see Supporting Information Table S1 C-RCS for curve metrics). Model comparisons between the C-RCS model and an intercept-only model show variable significance with age-dependent differences, likely due to increased inter-subject variability in older age groups (see Supporting Information Table S2 and Section 4). The covariate-adjusted restricted cubic spline was chosen because (a) it is a flexible fitting method that can represent a range of fits from linear to cubic and is consequently uniquely suited for brain volume data, which has notable variability in linearity across structures and developmental periods (as discussed in Hedman, van Haren, Schnack, Kahn, and Hulshoff Pol (2012) and Sowell et al. (2003)), (b) the use of the same model allows for cross-age comparisons, and (c) the use of the model allows us to account for known error in the data (i.e., field strength and sex), that is not appropriately accounted for in an intercept-only model. Notably, these benefits are not reflected in F-statistic model comparisons. Thus, while the C-RCS may not significantly out-perform the null in certain networks at certain ages, a priori knowledge strongly suggests it is the appropriate model fit for cross-age comparisons. The primary concern of splines, that is, overfitting, is addressed by the large number of subjects within each age bin (please see Table 1).

In order to examine nonlinear differences across populations, separate models were run for each developmental age group (also accounting for sex and field strength). Modeling independent curves for each age bin allowed for the independence assumption to be met in the Wilcoxon rank sum comparison (described below), and also acknowledged the cross-sectional nature of the data. For each volumetric trajectory, the 95% CI was derived by deploying C-RCS regression on 1,000 bootstrap samples (see Supporting Information Table S1 for average upper and lower CI values). The primary interest of the present study was to identify correlations between network growth curves (i.e., the model fits of each network). Consequently, within each age bin, pairwise correlations between each network's C-RCS curve was determined, and hierarchical clustering was performed to determine groups of networks that were most closely correlated. The Silhouette clustering algorithm was used to identify clusters of networks with the highest correlation (Rousseeuw, 1987). The Silhouette algorithm identifies clusters with maximum tightness within the cluster, and maximum separation from other clusters. Specifically, the Silhouette algorithm iteratively tests different partitions of a dendrogram and identifies the most efficient partition. For instance, for an assumed $k = 3$ clusters, the average distance between a single node (e.g., network) and all other nodes in the same cluster is calculated (this is a measure of cohesion, *A*). Then the average distance between the node and all points in the nearest cluster is calculated (this is a measure of separation from the closest other cluster, *B*). The Silhouette coefficient for a single node is then defined as the differences between *B* and *A*, divided by the max (*A*, *B*). This calculation is repeated for multiple k values, and the value with the highest silhouette coefficient is chosen.

2.6 | Modularity and organization metrics

The current literature on SCNs suggests that the relationship between modularity and organization may reflect critical age-dependent changes in gray matter. In the current article, modularity is defined as the degree to which networks form preferred sub-groupings of similar growth curve profiles. Specifically, for each age group, mean within-cluster distance values and mean between-cluster distance values were derived per network. The ratio of between: within distance was then calculated and scaled from 0 to 1, with a higher between : within distance ratio equal to higher modularity. Median network modularity was then compared across age groups using Wilcoxon rank sum tests. In one instance, the CB did not cluster with other networks

(in 7–12 year olds), and this network's modularity value was excluded from the analysis.[1] The formation of sub-groups along the continuum of modularity can either reflect *organized* or *disorganized* structural processes. One critical dimension of neural organization and health is the preservation of synchronization across homotopic brain regions (e.g., lateral coordination; LC; Luo et al., 2015; Shen et al., 2015; Tang et al., 2016; Wang et al., 2015). In this study, LC was defined as the median homotopic network correlations, normalized by the median inter-network correlations, with higher values signifying higher LC. Values were additional scaled by the maximum LC across age groups (e.g., values adjusted to 0–1 relative scale). Parcellation patterns of networks into sub-groups is another dimension of whether modularity is organized or disorganized. As stated above, parcellations were defined using the Silhouette clustering algorithm, which identifies clusters independently from the mean inter-network modularity.

2.7 | Age bins

Age groups (and knots for lifetime curves) were determined based on previously identified developmental shifts, specifically corresponding with transitions between childhood (7–12), late adolescence (12–19), young adulthood (19–30), middle adulthood (30–55), older adulthood (55–75), and late life (75–90; age bins are inclusive of youngest age). These age distinctions have been found to map onto developmental shifts in brain growth trajectories. Whole brain volume increases during childhood until early adolescents (~12 years old), followed by a steady decrease in whole brain volume until young adulthood (~18 years old); young adulthood (18 to ~30) is characterized by relative stability in brain volume, and a potential secondary wave of growth (Hedman et al., 2012). In the fourth decade, there is a peak in adult brain growth and white matter integrity (with some regional variabilty; Hedman et al., 2012; Westlye et al., 2010b), followed by accelerating decline into older adulthood. Older adults (~60) demonstrate a steady decline in brain volume, as well as a reduction in structural covariance across brain regions (Alexander-Bloch et al., 2013; Hedman et al., 2012), and this decline continues into later life (e.g., middle-old and oldest-old age groups: ~75 and older) (Resnick, Pham, Kraut, Zonderman, & Davatzikos, 2003). In the current study, we extended the older adult window to include 55–75, due to findings that suggest certain cortical regions show a slightly earlier trajectory shift (Sowell, Thompson, & Toga, 2004; Westlye et al., 2010a).

3 | RESULTS

Wilcoxon rank sum tests revealed significant differences in median modularity at key points across the lifespan (see Table 3 and Figure 4). This included significant modularity differences between childhood and adolescence (z = 3.0732; p = .0021); young and middle adulthood (z = 2.9744; p = .0029); and older adulthood and late life (z = −2.6154; p = .0089). Childhood was marked by the highest median modularity across networks, and middle adulthood marked by the lowest median modularity. Shifts in modularity were further characterized by the degree of lateral coordination (LC; see Table 3 and Figure 4) and parcellation patterns (see Figure 5). For a full list of curve metrics see Supporting Information Table S1.

[1]Inclusion of the CB with a modularity value of 0 did not change the significance of the age group comparisons.

TABLE 3 Modularity and lateral coordination measures per age bin

Age	Modularity			LC (median)	LC scaled
	x	*p* value	*z* value		
7–12	0.40	–	–	3.83	0.62
12–19	0.13	.00	3.07	5.82	0.94
19–30	0.13	.31	−1.03	6.16	1.00
30–55	0.05	.00	2.97	1.57	0.25
55–75	0.09	.15	−1.44	2.75	0.45
75–90	0.20	.01	−2.62	1.12	0.18

Significance determined from Wilcoxin rank sum tests comparing the medians of adjacent age groups. LC scores reported as median value across networks and LC value scaled to maximum LC across age groups.

Childhood (7–11.9 years): In childhood, median inter-network modularity was the highest across the lifespan, and significantly higher than adolescents. Networks were organized into functionally and structurally grouped parcellations, with high preservation of structural relationships across homotopic networks (e.g., high LC). All networks demonstrated decline across the age range, though the rate and shape of this decline differed across network clusters:

- Cluster 1 was a DMN and sensorimotor cluster (including bilateral sensorimotor, bilateral anterior, and posterior DMN, and right visual networks). Networks showed a steep, nonlinear declined across the entire age range, and this decline attenuated at ~9.5 years.
- Cluster 2 was a bilateral ACC cluster, which remained relatively stable across the age group.
- Cluster 3 was a sensory cluster (including bilateral auditory and left visual networks), which showed accelerating decline across the age range.
- Cluster 4 consisted of the CB, which increased in volume until ~ 8.7 years, then declined for the remainder of the age range.

Adolescence (12–18.9 years): Adolescence was marked by low modularity, as well as an increase in LC from childhood. This pattern was driven by homogenous decline (potentially due to pruning mechanisms; see Section 4) across all networks. Average network decline was the greatest across the lifespan (*mean network GMV decline* = ~40% lifetime decline), and, consistent with previous regional studies (Hedman et al., 2012) the range and shape of decline differed primarily across frontal versus nonfrontal structures:

- Cluster 1 consisted primarily of nonfrontal structures (bilateral visual, bilateral auditory, posterior DMN), and right ACC. These networks demonstrated linear decline across the age range.
- Cluster 2 consisted primarily of frontal structures and the spatially proximal sensory parietal strip (bilateral sensorimotor, bilateral anterior DMN, left ACC), and CB. These networks showed nonlinear decline, including attenuation from ~13.5 to 15.5 years.

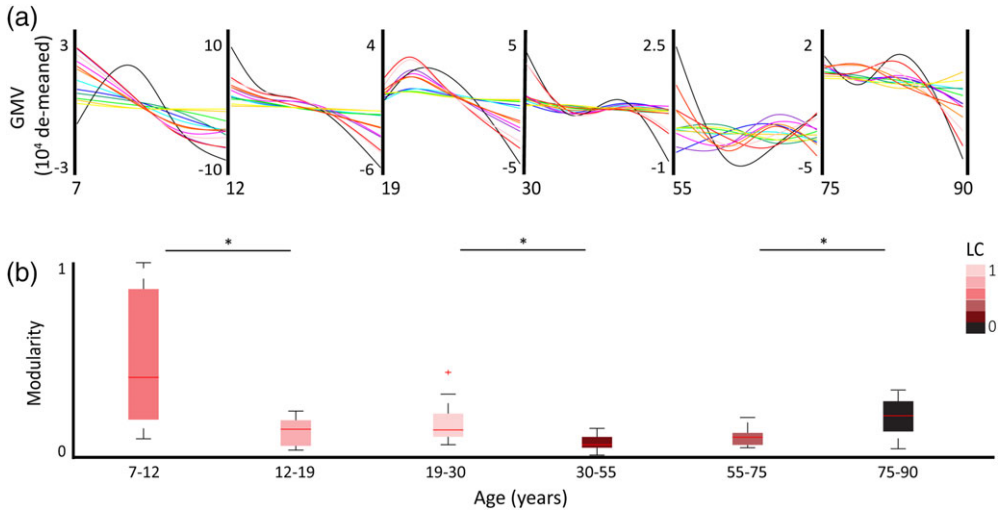

FIGURE 4 Network covariance trajectories across the lifespannetwork covariance trajectories across the lifespan. (a) De-meaned GMV growth curves per age bin for 13 networks. The network color legend is as follows: left visual (dark blue), right visual (cyan), left auditory (dark green), right auditory (light green), left sensorimotor (dark purple), right sensorimotor (light purple), cerebellum (black), left anterior cingulate (dark yellow), ¬¬right anterior cingulate (light yellow), left anterior default mode network (DMN; red), right anterior DMN (pink), left posterior DMN (orange), right posterior DMN (dark orange). (b) Box plots of inter-network modularity metrics per age bin. Box color represents the age bin's lateral coordination (LC) measure (scaled to group maximum). Significant differences in modularity were seen between children and adolescence; young and middle adults; and older adults and later life adults (indicated by asterisk [*]). See Table 3 for modularity and LC metrics, and Supporting Information Table S1 for growth curve values [Color figure can be viewed at wileyonlinelibrary.com]

Young adulthood (19–29.9 years): The adolescent pattern of low modularity and high LC continued into young adulthood, with notable uniformity among network growth curves, including the highest LC across the lifespan. Networks exhibited early increases until around 21 years (as seen in whole brain studies; see Hedman et al., 2012 for overview), followed by decreases until 30. Networks were differentiated by the rate and vertex of decline:

- Cluster 1 consisted of bilateral ACC, which demonstrated a relatively stable trajectory across the age range, with a slight increase until 21 years, followed by decline.
- Cluster 2 consisted of the majority of networks (including bilateral auditory and sensorimotor networks, bilateral anterior and posterior DMN, and the left visual network), which showed steep increases in volume until ~21 years, followed by linear decline through 30;
- Cluster 3 included the right visual network and CB, which showed increases in volume until ~22 years, followed by decline through 30.

Middle adulthood (30–54.9 years): Middle adulthood was marked by a significant reduction in modularity, as well as a general reduction in inter-network correlations and LC. While the curve variability was significantly higher across all networks in middle adulthood compared to earlier age groups, growth curves generally fell within two clustering patterns:

- Cluster 1 included bilateral auditory, bilateral ACC, CB networks, as well as bilateral anterior DMN and right posterior DMN. These networks demonstrated largely nonlinear decreases over the age range, with several (CB, bilateral anterior DMN, right posterior DMN, left ACC) showing attenuation between ~38 and 45 years, before continued decline to 55 years.
- Cluster 2 consisted of bilateral visual and sensorimotor networks and left posterior DMN, which showed decreases until ~38 years, followed by attenuation or increases until 55.

Notably, middle adulthood marked the first segregation of networks related to the DMN in adulthood (e.g., left posterior DMN separated from anterior DMN and right posterior DMN), as well as general separation of frontal-visual and frontal-parietal networks.

Older adulthood (55–74.9 years): Older adulthood exhibited a continuation of low inter-network modularity, and was additionally marked by low LC. Parcellations did not clearly reflect functional or structural groupings. Growth curves were characterized by considerable heterogeneity, which could be indicative of increased inter-individual variability (see Section 4). Within the context of this high curve variability, networks could generally be described by one of four growth curve patterns:

- Cluster 1 included anterior DMN and CB, which all decreased until ~65 years, followed by increases until 75 years.
- Cluster 2 included bilateral auditory and ACC networks, which showed relative stability across the age range, with each demonstrating decreases between ~58 and 70 years.
- Cluster 3 included the right visual network and bilateral posterior DMN. These networks each showed increases from ~60 to 70 years, followed by decline.
- Cluster 4 included left visual and bilateral sensorimotor networks, which all exhibited decreases until 62 years, attenuation/increase until 68 years, then decrease until 75 years.

Similar to middle adulthood, older adulthood reflected segregation of the DMN (e.g., anterior versus posterior DMN), as well as

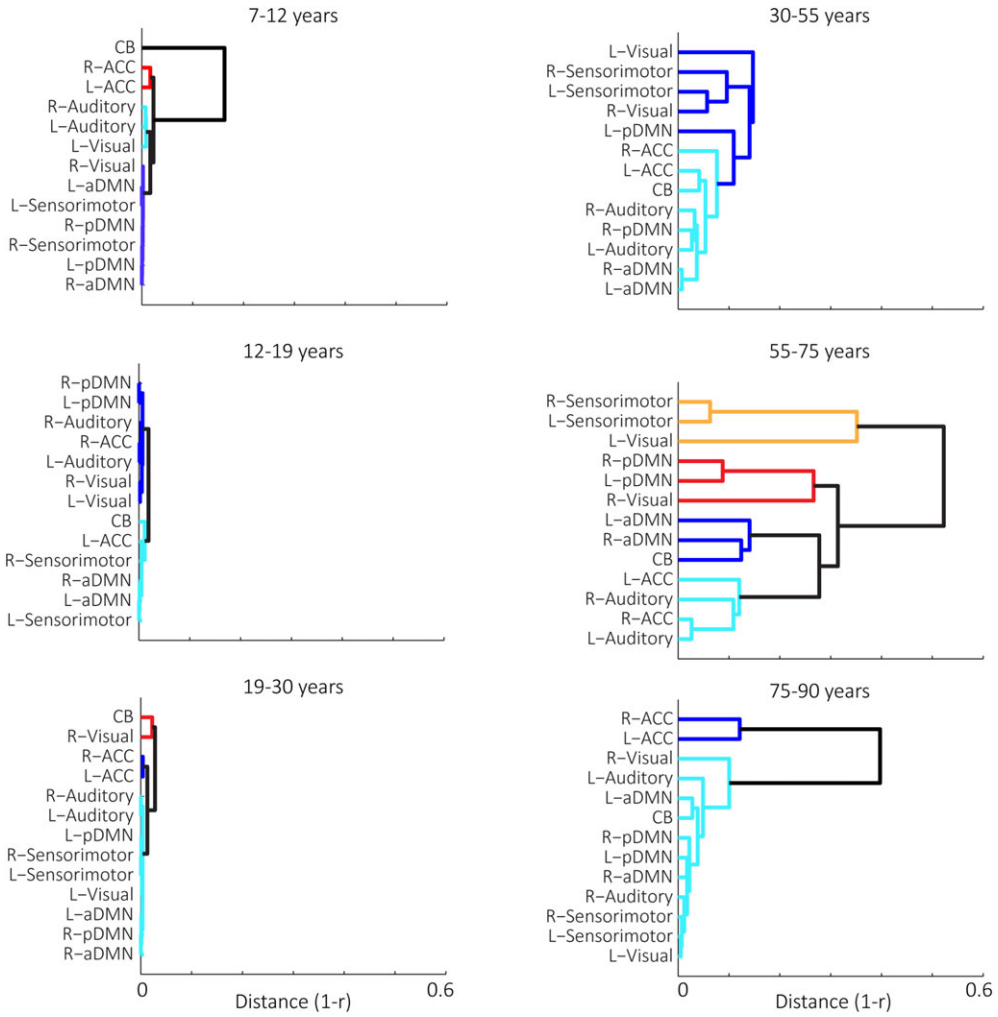

FIGURE 5 Network clustering patterns across the lifespannetwork hierarchical clustering patterns across the lifespan. Dendrograms demonstrate different hierarchical clustering patterns of network trajectories per age group. Clusters were identified through the Silhouette algorithm and are represented by different colors [Color figure can be viewed at wileyonlinelibrary.com]

separation of frontal-visual and frontal-parietal networks, as first seen in middle adulthood.

Late life (75–90 years): Late life networks showed significantly higher modularity than older adulthood, reflecting less clusters than other adult age groups due to unified decline across the majority of networks. Unlike the other age range with high modularity (childhood), underlying inter-network coupling patterns in late life demonstrated the lowest LC of the lifespan, suggesting underlying network disorganization in the decline. Each cluster showed unique growth trajectories:

- Cluster 1 included bilateral ACC, which showed relative stability across the age range.
- Cluster 2 included all other networks, which demonstrated a decreases across the age range. The point of shifting from stability to decrease, and the rate of decrease, varied by network.

4 | DISCUSSION

Structural covariance of brain networks provides insight into the typical and pathological brain (Alexander-Bloch et al., 2013; Evans, 2013), and allows for global markers of development and aging. The current study used a big-data framework and novel fitting approach to examine, for the first time, characteristics of inter-network structural covariance across the lifespan in typically developing and aging populations. We found that development and aging are characterized by key changes in volumetric inter-network relationships. Specifically, the degree to which network growth preferentially corresponded with other networks' growth, that is, modularity, significantly shifted at key developmental stages. Modularity changes were additionally characterized by unique, age-related parcellation patterns and the degree of homotopic coordination (LC), ultimately reflecting age-related alterations in inter-network organizational efficiency. In particular, childhood was the period of highest efficiency, while middle adulthood marked a drastic shift to decreased efficiency that continued through older adulthood.

Previous developmental studies of regional covariance suggest that brain organization shifts from localized topologies in childhood to more distributed topologies in young adulthood (Fair et al., 2009). And indeed, the findings in the current study demonstrate that this shift can additionally be seen at the level of inter-network relationships. Childhood showed preferred groupings between both spatially related

networks (e.g., anterior DMN and sensorimotor networks) and functionally related networks (e.g., anterior and posterior DMN), with a notable segregation between higher-level versus primary sensory networks (as seen in regional studies) (Khundrakpam et al., 2012). The high inter-network correlation values within certain clusters could signify a unique age-related network configuration, for example, the correlation between anterior and posterior nodes of the DMN could indicate that the DMN is a single structural unit in this younger age group instead of being segregated, as seen in older age groups (see below). These findings mark childhood as having higher inter-network "preference" within segregated clusters. This is as opposed to the significant shift to lower (but still organized) modularity in adolescence and young adulthood, marking more distributed growth relationships across all networks.

The shift from childhood to adolescence is marked by a significant transition into the most highly unified trajectories across the lifespan (e.g., high LC). Adolescent networks showed the greatest decline of the lifespan, and frontal decline was distinctly less linear than primary sensory networks and posterior associative structures in the DMN (Sowell et al., 2003). Because all networks were closely correlated in their decline, modularity for the age range was significantly lower than that seen in childhood, indicating that inter-network preferences were overwhelmed by homogenous, global brain processes. These findings are consistent with previous results that adolescence is marked by global, controlled synaptic pruning processes (Arain et al., 2013), which support reorganization of the brain into organized adult network patterns (Zielinski et al., 2010). And indeed, young adulthood saw a continuation of homogenous, organized growth across networks, with networks demonstrating a unified surge of growth from 19 to 21 followed by decline (Hedman et al., 2012).

As opposed to early life, patterns of volumetric decline in middle adulthood were marked by a significant reduction of inter-network modularity—a trend continued into older adulthood. The low modularity in both middle and older adulthood was marked by low LC, and disorganized network clustering patterns. Cluster disorganization included segregation of (a) networks related to the default mode, and (b) frontal networks from occipital and parietal networks. Additionally, during middle and older adulthood, the coordination between left and right frontal networks (e.g., anterior DMN, ACC, and sensorimotor) was maintained, while homotopic coordination of posterior structures was not (e.g., visual and posterior DMN). These findings are consistent with previous work showing decreased DMN integrity within aging (Andrews-Hanna et al., 2007; Siman-Tov et al., 2016), and increased isolation of frontal from other structures without reduced integrity of homotopic frontal communication (Chen et al., 2011). More generally, these results for middle and older adulthood add to functional evidence that aging is marked by desegregation—that is, a decrease in specific network coupling and an increase in inter-network communication (Chan et al., 2014; Chen et al., 2011; Siman-Tov et al., 2016). These findings extend results in functional MRI studies on aging, which suggest that the shift from intra- to inter-network communication reflects despecialization of function within brain areas and a resulting compensatory inter-network "cross-talk" to support regions with degraded functions (Brier et al., 2014; Chan et al., 2014). Specifically, patterns of desegregation, as measured by functional differences in modularity, show negative associations with memory in aging (Chan et al., 2014), and for some networks, have also been suggested to be potential biomarkers for neurodegenerative diseases (Hohenfeld et al., 2018). Future studies should use the present framework to examine patterns of inter-network modularity in clinical populations (see Section 5).

An additional dimension of the overall disorganization in middle and older adulthood is high curve variability, which likely reflects, in part, greater inter-subject variability across time points. In this context, our results are consistent with a long history of both longitudinal and cross-sectional cognitive literature that suggest older age groups are the most heterogeneous populations across the lifespan, with increased within- and between-subject variability (Hultsch et al., 2002; Nelson et al., 1992). Though the influence of inter-subject variability is certainly a limitation of cross-sectional observations (see Section 5), increased variability also reflects important changes in the population norm of these age groups. As opposed to early and late life, in which biological imperatives of growth and decline overwhelm inter-individual differences (e.g., as reflected by our findings of global volumetric decline with minimal preservation of homotopic or functional connections) (Fotenos, Mintun, Snyder, Morris, & Buckner, 2008; Lemaitre et al., 2012; Resnick et al., 2003; Westlye et al., 2010a) our results suggest that middle and older adulthood are developmental periods in which subpopulation differences could be most influential, even within typical cohorts without cognitive impairment.

Our findings consequently point to specific, age-related patterns of inter-network modularity and organization across the lifespan that likely reflect both individual and population-level characteristics: the organization of childhood network growth could be seen to reflect both expected individual growth patterns as well as relative homogeneity at the population-level, as compared to later life in which the disorganization seen in middle and older adulthood may reflect both individual and population variability (see Section 5).

5 | LIMITATIONS AND FUTURE DIRECTIONS

The current study has several limitations. In order to take advantage of the big-data framework across the entire lifespan, specific site was not included as a regressor. Controlling for study-related variance is a key difficulty in big-data approaches (as discussed in Coupé, Catheline, Lanuza, & Manjón, 2017). Because study correlates with age, controlling for study would reduce the age effect. Additionally, controlling for study reduces statistical power, effectively diminishing the gain of combining studies to look at an unprecedented number of images. However, we have taken the following steps to minimize study effects on the present findings: (a) we used a segmentation algorithm that is robust to study-related intensity differences (b) we controlled for magnet strength, which is a primary contributor of study-related differences in T1 images (Han et al., 2006), (c) we performed manual and automated QC pipelines to ensure appropriate segmentation of all images, (d) we ensured that each age bin is represented by a minimum of five studies, and (e) we ensured that each study contributes to a minimum of three age bins. These steps are

comparable to other big-data studies facing a similar problem (Coupé et al., 2017). Notably, previous studies have found that the impact of scanner manufacturer, magnet strength, and their interaction on gray matter volume measurements is limited in big-data environments, with the majority of variance explained by TICV, age, and sex (Potvin, Dieumegarde, & Duchesne, 2017; Potvin, Mouiha, Dieumegarde, & Duchesne, 2016). Second, the current study is a cross-sectional design rather than longitudinal. Future longitudinal studies are needed to distinguish individual versus population patterns. Last, due to (a) the cross-sectional nature of the data and (b) the need for independent growth curves to meet assumption criteria in the statistical comparisons across age groups, the current study modeled growth curves independently for each age bin. This results in noncontinuous curves at the age bin edges (please see Supporting Information Figure S2), and potential model fit differences based on differing age bin widths. To minimize curve edge-effects, this study employed a restricted cubic spline model, however in the ideal data scenario (i.e., longitudinal data), brain growth would be treated continuously across the lifespan.

This study is the first to comprehensively identify inter-network covariance patterns across the lifespan. Future studies should extend the current approach to measures of cortical thickness and surface area, and use the presented metrics to examine neurobiologically vulnerable populations, such as those from low socioeconomic backgrounds and those at risk for neurodegenerative disease. While the current study aimed to quantitatively compare inter-network interactions across networks known to be replicable within and across age groups, future studies should (a) employ complimentary data-driven approaches to replicate and extend the present findings, and (b) examine interactions between intra- and inter-network relationships using a region- rather than network-based parcellation. Additional longitudinal studies are also needed to specifically identify individual- versus population-based trajectories. Through our novel examination of structural network coordination, the current study pushes toward a connectomics viewpoint of aging and development, and sets the groundwork for identifying age-sensitive, system-level biomarkers for disease states across the lifespan.

ACKNOWLEDGMENTS

We would like to thank all of the participants that made this work possible. Additionally, we'd like to thank and acknowledge the open access data platforms and data sources that were used for this work, including: XNAT, Neuroimaging Informatics Tool and Resources Clearinghouse (NITRC), 1000 Functional Connectomes Project (fcon-1000), Autism Brain Imaging Data Exchange (ABIDE I), Attention Deficit Hyperactivity Disorder 200 (ADHD-200), Baltimore Longitudinal Study of Aging (BLSA), Education and Brain sciences Research Lab (EBRL), Information eXtraction from Images (IXI; http://brain-development.org/ixi-dataset), National Database for Autism Research (NDAR; NIH MRI Study of Normal Brain Development, dataset #1151; http://www.bic.mni.mcgill.ca/nihpd/info/participating_centers.html), Nathan Kline Institute Rockland Sample (NKI Rockland), and Open Access Series of Imaging Studies (OASIS). This research was conducted with the support from the Intramural Research Program, National Institute on Aging, NIH. The current work was additionally made possible by the following grants: NSF CAREER 1452485 (Landman), NIH R01EB017230 (Landman), NIH R21EY024036 (Landman), NIH R21NS064534 (Prince/Landman), NIH R03EB012461 (Landman), R01 HD067254 (Cutting), R01 HD044073 (Cutting), U54 HD083211 (Dykens/Cutting), NCATS/NIH UL1 TR000445 (Vanderbilt CTSA). The NIH MRI Study of Normal Brain Development is supported by the National Institute of Child Health and Human Development, the National Institute on Drug Abuse, the National Institute of Mental Health, and the National Institute of Neurological Disorders and Stroke— Contract #s N01-HD02-3343, N01-MH9-0002, and N01-NS-9-2314, N01-NS-9-2315, N01-NS-9-2316, N01-NS-9-2317, N01-NS-9-2319 and N01-NS-9-2320. This manuscript reflects the views of the authors and may not reflect the opinions or views of the NIH. Additional funding sources can be found at: http://fcon_1000.projects.nitrc.org/fcpClassic/FcpTable.html (1000 Functional Connectomes Project); http://fcon_1000.projects.nitrc.org/indi/abide/abide_I.html (ABIDE); http://fcon_1000.projects.nitrc.org/indi/adhd200/ (ADHD-200); http://fcon_1000.projects.nitrc.org/indi/enhanced/ (NKI Rockland); http://www.oasis-brains.org/ (OASIS).

CONFLICT OF INTEREST

The authors have no biomedical financial interests or potential conflicts of interest.

ORCID

Laurie E. Cutting https://orcid.org/0000-0002-2362-6028

REFERENCES

Alexander-Bloch, A., Giedd, J. N., & Bullmore, E. (2013). Imaging structural co-variance between human brain regions. *Nature Reviews. Neuroscience*, *14*(5), 322–336. http://doi.org/10.1038/nrn3465

Alexander-Bloch, A., Raznahan, A., Bullmore, E., & Giedd, J. (2013). The convergence of maturational change and structural covariance in human cortical networks. *The Journal of neuroscience : The Official Journal of the Society for Neuroscience*, *33*(7), 2889–2899. http://doi.org/10.1523/JNEUROSCI.3554-12.2013

Andrews-Hanna, J. R., Snyder, A. Z., Vincent, J. L., Lustig, C., Head, D., Raichle, M. E., & Buckner, R. L. (2007). Disruption of large-scale brain systems in advanced aging. *Neuron*, *56*(5), 924–935. http://doi.org/10.1016/j.neuron.2007.10.038

Arain, M., Haque, M., Johal, L., Mathur, P., Nel, W., Rais, A., … Sharma, S. (2013). Maturation of the adolescent brain. *Neuropsychiatric Disease and Treatment*, *9*, 449–461. http://doi.org/10.2147/NDT.S39776

Avants, B. B., Epstein, C. L., Grossman, M., & Gee, J. C. (2008). Symmetric diffeomorphic image registration with cross-correlation: evaluating automated labeling of elderly and neurodegenerative brain. *Medical Image Analysis*, *12*, 26–41. [PubMed: 17659998]

Barnes, J., Ridgway, G. R., Bartlett, J., Henley, S. M., Lehmann, M., Hobbs, N., … Fox, N. C. (2010). Head size, age and gender adjustment in MRI studies: a necessary nuisance? *Neuroimage*, *53*, 1244–1255. https://doi.org/10.1016/j.neuroimage.2010.06.025

Bermudez, P., Lerch, J. P., Evans, A. C., & Zatorre, R. J. (2009). Neuroanatomical correlates of musicianship as revealed by cortical thickness and voxel-based morphometry. *Cerebral Cortex (New York, N.Y. : 1991)*, *19*(7), 1583–1596. http://doi.org/10.1093/cercor/bhn196

Brier, M. R., Thomas, J. B., Fagan, A. M., Hassenstab, J., Holtzman, D. M., Benzinger, T. L., … Ances, B. M. (2014). Functional connectivity and graph theory in preclinical Alzheimer's disease. *Neurobiology of Aging*, *35*(4), 757–768. http://doi.org/10.1016/j.neurobiolaging.2013.10.081

Chan, M. Y., Park, D. C., Savalia, N. K., Petersen, S. E., & Wig, G. S. (2014). Decreased segregation of brain systems across the healthy adult lifespan. *Proceedings of the National Academy of Sciences of the United States of America*, *111*(46), E4997–E5006. http://doi.org/10.1073/pnas.1415122111

Chen, Z. J., He, Y., Rosa-Neto, P., Gong, G., & Evans, A. C. (2011). Age-related alterations in the modular organization of structural cortical network by using cortical thickness from MRI. *NeuroImage*, *56*(1), 235–245. http://doi.org/10.1016/j.neuroimage.2011.01.010

Coupé, P., Catheline, G., Lanuza, E., & Manjón, J. V. (2017). Towards a unified analysis of brain maturation and aging across the entire lifespan: A MRI analysis. *Human Brain Mapping*, Nov; 38(11). http://doi.org/10.1002/hbm.23743

Evans, A. C. (2013). Networks of anatomical covariance. *NeuroImage*, *80*, 489–504. http://doi.org/10.1016/j.neuroimage.2013.05.054

Fair, D. A., Cohen, A. L., Power, J. D., Dosenbach, N. U. F., Church, J. A., Miezin, F. M., … Petersen, S. E. (2009). Functional brain networks develop from a "local to distributed" organization. *PLoS Computational Biology*, *5*(5), e1000381. http://doi.org/10.1371/journal.pcbi.1000381

Farias, S. T., Mungas, D., Reed, B., Carmichael, O., Beckett, L., Harvey, D., … DeCarli, C. (2012). Maximal brain size remains an important predictor of cognition in old age, independent of current brain pathology. *Neurobiol Aging*, *33*, 1758–1768. https://doi.org/10.1016/j.media.2007.06.004

Fotenos, A. F., Mintun, M. A., Snyder, A. Z., Morris, J. C., & Buckner, R. L. (2008). Brain volume decline in aging: Evidence for a relation between socioeconomic status, preclinical Alzheimer disease, and reserve. *Archives of Neurology*, *65*(1), 113–120. http://doi.org/10.1001/archneurol.2007.27

Geng, X., Li, G., Lu, Z., Gao, W., Wang, L., Shen, D., … Gilmore, J. H. (2016). Structural and maturational covariance in early childhood brain development. *Cerebral Cortex*, *27*(3), bhw022. http://doi.org/10.1093/cercor/bhw022

Gogtay, N., Giedd, J. N., Lusk, L., Hayashi, K. M., Greenstein, D., Vaituzis, A. C., … Thompson, P. M. (2004). Dynamic mapping of human cortical development during childhood through early adulthood. *Proceedings of the National Academy of Sciences of the United States of America*, *101*(21), 8174–8179. http://doi.org/10.1073/pnas.0402680101

Gong, G., Rosa-Neto, P., Carbonell, F., Chen, Z. J., He, Y., & Evans, A. C. (2009). Age- and gender-related differences in the cortical anatomical network. *Journal of Neuroscience*, *29*(50), 15684–15693. http://doi.org/10.1523/JNEUROSCI.2308-09.2009

Guo, X., Wang, Y., Guo, T., Chen, K., Zhang, J., Li, K., … Yao, L. (2015). Structural covariance networks across healthy young adults and their consistency. *Journal of Magnetic Resonance Imaging*, *42*(2), 261–268. http://doi.org/10.1002/jmri.24780

Han, X., Jovicich, J., Salat, D., van der Kouwe, A., Quinn, B., Czanner, S., … Fischl, B. (2006). Reliability of MRI-derived measurements of human cerebral cortical thickness: The effects of field strength, scanner upgrade and manufacturer. *NeuroImage*, *32*(1), 180–194. http://doi.org/10.1016/J.NEUROIMAGE.2006.02.051

Harrell, F. E. J. (2015). *Regression Modeling Strategies with Applications to Linear Models, Logistic Regression, and Survival Analysis* (2nd ed.). New York: Springer.

Hedman, A. M., van Haren, N. E. M., Schnack, H. G., Kahn, R. S., & Hulshoff Pol, H. E. (2012). Human brain changes across the life span: A review of 56 longitudinal magnetic resonance imaging studies. *Human Brain Mapping*, *33*(8), 1987–2002. http://doi.org/10.1002/hbm.21334

Hohenfeld, C., Werner, C. J., & Reetz, K. (2018). Resting-state connectivity in neurodegenerative disorders: Is there potential for an imaging biomarker? *NeuroImage Clinical*, *18*, 849–870. http://doi.org/10.1016/j.nicl.2018.03.013

Huo, Y., Aboud, K., Kang, H., Cutting, L. E., & Landman, B. A. (2016). Mapping Lifetime Brain Volumetry with Covariate-Adjusted Restricted Cubic Spline Regression from Cross-sectional Multi-site MRI. *Medical Image Computing and Computer-Assisted Intervention : MICCAI ... International Conference on Medical Image Computing and Computer-Assisted Intervention*, *9900*, 81–88. http://doi.org/10.1007/978-3-319-46720-7_10

Hultsch, D. F., MacDonald, S. W. S., & Dixon, R. A. (2002). Variability in reaction time performance of younger and older adults. *The Journals of Gerontology. Series B, Psychological Sciences and Social Sciences*, *57*(2), 101–115. http://doi.org/10.1093/GERONB/57.2.P101

Klein, A., Dal Canton, T., Ghosh, S. S., Landman, B., Lee, J., & Worth, A. (2010). *Open labels: online feedback for a public resource of manually labeled brain images*. 16th Annual Meeting for the Organization of Human Brain Mapping.

Khundrakpam, B. S., Reid, A., Brauer, J., Carbonell, F., Lewis, J., Ameis, S., … O'Neill, J. (2012). Developmental changes in organization of structural brain networks. *Cerebral Cortex*, *23*(9), 2072–2085. http://doi.org/10.1093/cercor/bhs187

La, C., Mossahebi, P., Nair, V. A., Bendlin, B. B., Birn, R., Meyerand, M. E., & Prabhakaran, V. (2015). Age-related changes in inter-network connectivity by component analysis. *Frontiers in Aging Neuroscience*, *7*, 237. http://doi.org/10.3389/fnagi.2015.00237

Lemaitre, H., Goldman, A. L., Sambataro, F., Verchinski, B. A., Meyer-Lindenberg, A., Weinberger, D. R., & Mattay, V. S. (2012). Normal age-related brain morphometric changes: Nonuniformity across cortical thickness, surface area and gray matter volume? *Neurobiology of Aging*, *33*(3), 617.e1–617.e9. http://doi.org/10.1016/j.neurobiolaging.2010.07.013

Lerch, J. P., Worsley, K., Shaw, W. P., Greenstein, D. K., Lenroot, R. K., Giedd, J., & Evans, A. C. (2006). Mapping anatomical correlations across cerebral cortex (MACACC) using cortical thickness from MRI. *NeuroImage*, *31*(3), 993–1003. http://doi.org/10.1016/j.neuroimage.2006.01.042

Li, X., Pu, F., Fan, Y., Niu, H., Li, S., & Li, D. (2013). Age-related changes in brain structural covariance networks. *Frontiers in Human Neuroscience*, *7*, 98. http://doi.org/10.3389/fnhum.2013.00098

Liao, W., Zhang, Z., Mantini, D., Xu, Q., Wang, Z., Chen, G., … Lu, G. (2013). Relationship between large-scale functional and structural covariance networks in idiopathic generalized epilepsy. *Brain Connectivity*, *3*(3), 240–254. http://doi.org/10.1089/brain.2012.0132

Luo, C., Guo, X., Song, W., Zhao, B., Cao, B., Yang, J., … Shang, H.-F. (2015). Decreased resting-state interhemispheric functional connectivity in Parkinson's disease. *BioMed Research International*, *2015*, 692684. http://doi.org/10.1155/2015/692684

Lv, Y.-T., Yang, H., Wang, D.-Y., Li, S.-Y., Han, Y., Zhu, C.-Z., … Zang, Y.-F. (2008). Correlations in spontaneous activity and gray matter density between left and right sensoritmotor areas of pianists. *Neuroreport*, *19*(6), 631–634. http://doi.org/10.1097/WNR.0b013e3282fa6da0

Montembeault, M., Joubert, S., Doyon, J., Carrier, J., Gagnon, J.-F., Monchi, O., … Brambati, S. M. (2012). The impact of aging on gray matter structural covariance networks. *NeuroImage*, *63*(2), 754–759. http://doi.org/10.1016/j.neuroimage.2012.06.052

Nelson, A. E., & Dannefer, D. (1992). Aged heterogeneity: Fact or fiction? The fate of diversity in gerontological research. *Gerontologist*, *32*(1), 17–23. http://doi.org/10.1093/geront/32.1.17

Peelle, J. E., Cusack, R., & Henson, R. N. A. (2012). Adjusting for global effects in voxel-based morphometry: Gray matter decline in normal aging. *Neuroimage*, *60*, 1503–1516. https://doi.org/10.1016/j.neuroimage.2011.12.086

Potvin, O., Dieumegarde, L., & Duchesne, S. (2017). Freesurfer cortical normative data for adults using Desikan-Killiany-Tourville and ex vivo protocols. *NeuroImage*, *156*, 43–64. http://doi.org/10.1016/J.NEUROIMAGE.2017.04.035

Potvin, O., Mouiha, A., Dieumegarde, L., & Duchesne, S. (2016). Normative data for subcortical regional volumes over the lifetime of the adult human brain. *NeuroImage*, *137*, 9–20. http://doi.org/10.1016/J.NEUROIMAGE.2016.05.016

Resnick, S. M., Pham, D. L., Kraut, M. A., Zonderman, A. B., & Davatzikos, C. (2003). Longitudinal magnetic resonance imaging studies of older adults: A shrinking brain. *The Journal of Neuroscience*, *23*(8), 3295–3301. http://doi.org/23/8/3295 [pii].

Rousseeuw, P. J. (1987). Silhouettes: A graphical aid to the interpretation and validation of cluster analysis. *Journal of Computational and Applied Mathematics*, *20*, 53–65. http://doi.org/10.1016/0377-0427(87)90125-7

Seeley, W. W., Crawford, R. K., Zhou, J., Miller, B. L., & Greicius, M. D. (2009). Neurodegenerative diseases target large-scale human brain networks. *Neuron*, *62*(1), 42–52. http://doi.org/10.1016/j.neuron.2009.03.024

Shen, K., Mišić, B., Cipollini, B. N., Bezgin, G., Buschkuehl, M., Hutchison, R. M., … Berman, M. G. (2015). Stable long-range

interhemispheric coordination is supported by direct anatomical projections. *Proceedings of the National Academy of Sciences of the United States of America*, *112*(20), 6473–6478. http://doi.org/10.1073/pnas.1503436112

Siman-Tov, T., Bosak, N., Sprecher, E., Paz, R., Eran, A., Aharon-Peretz, J., & Kahn, I. (2016). Early age-related functional connectivity decline in high-order cognitive networks. *Frontiers in Aging Neuroscience*, *8*, 330. http://doi.org/10.3389/fnagi.2016.00330

Smith, S. M., De Stefano, N., Jenkinson, M., & Matthews, P. M. (2001). Normalized accurate measurement of longitudinal brain change. *Journal of Computer Assisted Tomography*, *25*(3), 466–475. http://doi.org/10.1097/00004728-200105000-00022

Smith, S. M., Zhang, Y., Jenkinson, M., Chen, J., Matthews, P. M., Federico, A., & De Stefano, N. (2002). Accurate, robust, and automated longitudinal and cross-sectional brain change analysis. *NeuroImage*, *17*(1), 479–489. http://doi.org/10.1006/nimg.2002.1040

Smith, S. M., Jenkinson, M., Woolrich, M. W., Beckmann, C. F., Behrens, T. E. J., Johansen-Berg, H., … Matthews, P. M. (2004). Advances in functional and structural MR image analysis and implementation as FSL. *NeuroImage*, *23*, S208–S219. http://doi.org/10.1016/J.NEUROIMAGE.2004.07.051

Sowell, E. R., Peterson, B. S., Thompson, P. M., Welcome, S. E., Henkenius, A. L., & Toga, A. W. (2003). Mapping cortical change across the human life span. *Nature Neuroscience*, *6*(3), 309–315. http://doi.org/10.1038/nn1008

Sowell, E. R., Thompson, P. M., & Toga, A. W. (2004). Mapping changes in the human cortex throughout the span of life. *The Neuroscientist*, *10*(4), 372–392. http://doi.org/10.1177/1073858404263960

Sporns, O., & Betzel, R. F. (2016). Modular brain networks. *Annual Review of Psychology*, *67*, 613–640. http://doi.org/10.1146/annurev-psych-122414-033634

Tang, C., Zhao, Z., Chen, C., Zheng, X., Sun, F., Zhang, X., … Jia, J. (2016). Decreased functional connectivity of homotopic brain regions in chronic stroke patients: A resting state fMRI study. *PLoS One*, *11*(4), e0152875. http://doi.org/10.1371/journal.pone.0152875

Tost, H., Bilek, E., & Meyer-Lindenberg, A. (2012). Brain connectivity in psychiatric imaging genetics. *NeuroImage*, *62*(4), 2250–2260. http://doi.org/10.1016/j.neuroimage.2011.11.007

Wang, Z., Wang, J., Zhang, H., Mchugh, R., Sun, X., Li, K., & Yang, Q. X. (2015). Interhemispheric functional and structural disconnection in Alzheimer's disease: A combined resting-state fMRI and DTI study. *PLoS One*, *10*(5), e0126310. http://doi.org/10.1371/journal.pone.0126310

Westman, E., Aguilar, C., Muehlboeck, J. S., & Simmons, A. (2013). Regional magnetic resonance imaging measures for multivariate analysis in Alzheimer's disease and mild cognitive impairment. *Brain Topogr*, *26*, 9–23. https://doi.org/10.1007/s10548-012-0246-x

Westlye, L. T., Walhovd, K. B., Dale, A. M., Bjørnerud, A., Due-Tønnessen, P., Engvig, A., … Fjell, A. M. (2010a). Differentiating maturational and aging-related changes of the cerebral cortex by use of thickness and signal intensity. *NeuroImage*, *52*(1), 172–185. http://doi.org/10.1016/j.neuroimage.2010.03.056

Westlye, L. T., Walhovd, K. B., Dale, A. M., Bjørnerud, A., Due-Tønnessen, P., Engvig, A., … Fjell, A. M. (2010b). Life-span changes of the human brain white matter: Diffusion tensor imaging (DTI) and volumetry. *Cerebral Cortex (New York, N.Y. : 1991)*, *20*(9), 2055–2068. http://doi.org/10.1093/cercor/bhp280

Whitwell, J. L., Crum, W. R., Watt, H. C., & Fox, N. C. (2001). Normalization of cerebral volumes by use of intracranial volume: implications for longitudinal quantitative MR imaging. *American Journal of Neuroradiology*, *22*, 1483–1489.

Zielinski, B. A., Gennatas, E. D., Zhou, J., & Seeley, W. W. (2010). Network-level structural covariance in the developing brain. *Proceedings of the National Academy of Sciences of the United States of America*, *107*(42), 18191–18196. http://doi.org/10.1073/pnas.1003109107

SUPPORTING INFORMATION

Additional supporting information may be found online in the Supporting Information section at the end of the article.

How to cite this article: Aboud KS, Huo Y, Kang H, et al. Structural covariance across the lifespan: Brain development and aging through the lens of inter-network relationships. *Hum Brain Mapp*. 2019;40:125–136. https://doi.org/10.1002/hbm.24359